❒ 86

A calculation method of the passive wireless surface acoustic wave sensor response phase

Nguyen Thu Ha[1,2], Trinh Van Thai[1], Thanh Long Cung[1], Hoang Si Hong[1]

[1]Department of Automation Engineering, School of Electrical and Electronic Engineering, Hanoi University of Science and Technology, Hanoi, Vietnam
[2]Faculty of Electrical Engineering Technology, Hanoi University of Industry, Hanoi, Vietnam

Article Info

ABSTRACT

In this research, we propose a method to calculate the phase delay angle of the reflected wave compared to the wave emitted from the interdigital transducer (IDT) of a passive wireless surface acoustic wave (SAW) sensor by combining simulation of the finite element method (FEM) and MATLAB. Based on the result, we consider the influence of the reflector position on the phase delay of the SAW sensor consisting of an IDT and three equally spaced reflectors. The distances between the IDT and the first reflector are 870 micrometers, 939.6 micrometers, and 1009.2 micrometers, and the distances between the reflector positions are 452.4 micrometers, 522 micrometers, and 591.6 micrometers. The outputs of the FEM simulation, including delay time, amplitude loss, and the length of the reflected wave are put into the model in MATLAB to determine the phase delay of the response waves. The obtained phase delay results show that as the distance between the IDT and the reflectors increases, the phase delay angle increases to 4.49 degrees, 5.39 degrees, and 5.78 degrees, respectively.

Corresponding Author:

Hoang Si Hong
Department of Automation Engineering, School of Electrical and Electronic Engineering
Hanoi University of Science and Technology
Dai-Co-Viet Street, Hai-Ba-Trung district, Hanoi, Vietnam
Email: hong.hoangsy@hust.edu.vn

1. INTRODUCTION

Surface acoustic wave (SAW) sensors are widely used in measurement and identification systems, and applied in different fields such as measuring high temperatures in harsh environmental conditions [1]–[3], pressure [4], [5], torque [6], [7], magnetic and humidity [8] or in identification tags (ID-tag) by their superiority as no battery or do not require any power supply to operate, wireless, small, made on highly stable materials. Using passive wireless SAW sensors requires a reader to transmit radio frequency (RF) signals and receive reflected signals that carry measurement information. Several publications have mentioned the reader of the passive wireless SAW sensor [9]–[14]. The previous authors [9] built a sensor network model with four wireless SAWs for industrial applications, used a network analyzer to read the reflected pulses and calculated the result on MATLAB software, but they did not mention the algorithms on the reader. Bruckner and Bardong [10], have investigated the reader architecture, methods of time-domain sampling (TDS), and frequency-domain sampling (FDS), in which the author also analyzed and proposed the theory of hybrid structure TDS/FDS for the reader, but the article has not mentioned the result of the simulation or experimental on the device. In the fabrication process of a SAW temperature sensor presented in [11], the authors used the results from the finite element method (FEM) and the boundary element method (BEM) simulation to fabricate sensors, but the computational solution to read the feedback pulse has not been mentioned.

Some experiments on a reader have been presented. According to Krishnamurthy *et al.* [12], the transmission and reception of the reader were separated by on/off the switching at 50 Khz. The transmitted and received signals are simulated with a relatively long reading period, making them unsuitable for highly dynamic measurements. The results published in [15] have indicated a method to calculate the phase delay between the reflected waves and interrogation signals of the SAW delay line sensor, thereby calculating the $tan\ \varphi$ (φ is the phase shift angle of reflected pulses) using a model on MATLAB software. However, the data input to the model was random values, which had been chosen to test the model and the $tan\varphi$ is not convenient for scale. In addition, the article did not consider the influence of reflectors. Research by Kozlovski *et al.* [16], built a reader to read the temperature of four SAW sensors at the same time, but the number of sensors was small and the manufacturing process was complicated, requiring a lot of experience to test the different properties of the sensor.

For passive wireless SAW sensors, the phase shift between interrogation signals and response pulses contains measurement informations [17]. The reader must capture the peak of the reflected wave in order to calculate the phase shift corresponding to the measurement. Studies [15], [17] have shown that the phase shift is affected by the measurand and shown the time delay between sending the probe pulse and receiving the reflected pulse. In addition, the position of the reflectors also affects the delay time of the reflected wave [18], so it is necessary to evaluate the position of the reflector with respect to the phase shift angle. In this study, we look at a specific way to figure out the phase angle directly from the delay time of the reflected pulse, and we also look at how the position of the reflector affects the phase shift.

Because of advantages such as easy device structure modeling, adaptability, and time-dependent simulation. FEM and MATLAB have been used by many researchers for design and simulation in various sensor fields. Kozlovski *et al.* [16], used MATLAB to program signal processing and temperature extraction in the 915 MHz correlator transceiver and sensor system. While using FEM to analyze and optimize a candidate ultra-wideband antenna for Ku-band wireless is mentioned in [19]. In this study, we use a combination of FEM simulation and MATLAB to simulate single-port SAW reflective delay line (RDL) structure on FEM with YZ-LiNbO$_3$ piezoelectric substrate. The outputs of the FEM simulation were imported into blocks in MATLAB to calculate the phase difference.

2. SIMULATION PROCESS

SAW device configurations include SAW delay line, one-port SAW resonator, and two-port SAW resonator. In this paper, the authors used the SAW RDL because they are commonly used for passive wireless sensing systems [20].

2.1. Principle of passive wireless SAW

Figure 1(a) shows the principle of the one-port SAW RDL and the phase difference of the reflected signals are shown in Figure 1(b). The system has two devices, the reader and the sensor. Where the sensor is a piezoelectric substrate on the surface put an interdigital transducer (IDT) and reflectors, and there is an antenna attached to the IDT, the reader also attached an antenna to transmit/receive electromagnetic signals. The reader emits interrogation pulses propagation to the antenna of the IDT. Here, the electrical signals are converted into acoustic waves and propagate on the surface of the piezoelectric substrate. When the acoustic waves propagate to the reflectors, a part of these waves will reflect in the IDT. The antenna will receive the reflected pulses and sends them back to the reader, where they should compute to determine the sensor's measurement values.
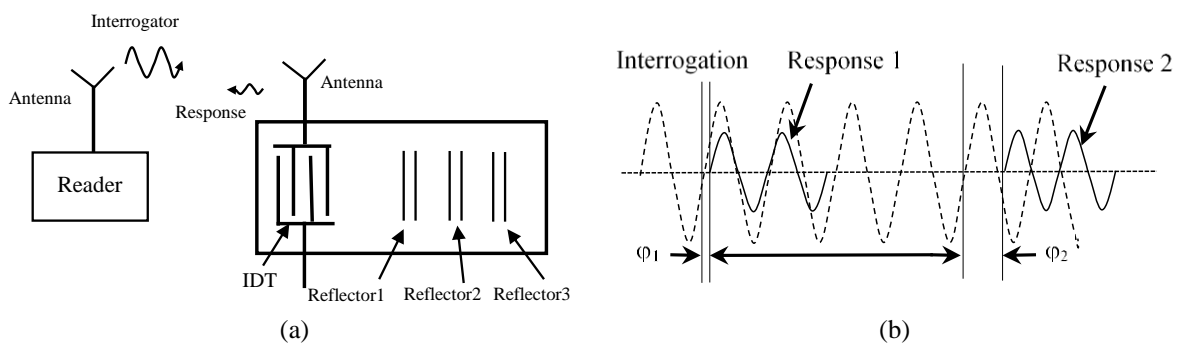

Figure 1. The one-port SAW RDL (a) the top view of the structure and (b) the phase difference between the response and the interrogation pulse

The propagation of SAWs depends on the geometry of the substrate and environmental conditions. In Table 1, the obtainable linear coefficients for physical effects on SAW substrates are summarized [21]. The response pulses from the reflectors provide the measurement informations. In Figure 1(b), φ_1 and φ_2 are the phase shift in the first and the second response, respectively, and the interrogation pulse. The propagation time of acoustic wave on the substrate is:

$$T_{Di} = \frac{L_i}{v_{saw}}$$ (1)

where L_i is the distance from IDT to the i_{th} reflector and v_{saw} is the velocity of SAWs.

In SAW sensor applications, L_i and v_{saw} are changed due to variations in temperature, mechanical stress, and strain on the surface layer.

Table 1. Linear coefficients for physical effects on SAW substrate materials [21]

Physical quantity	Linear coefficient
Temperature	Up to 100 ppm/K
Pressure, stress	2 ppm/kPa
Force	10 ppm/kN
Mass loading	30 ppm/μg.cm^2
Voltage	1 ppm/V
Electric field	30 ppm/V.μm

Reflectors are designed to a part of the incoming waves from the IDT will be reflected while the remainder will pass through and reach the next. The relative sensitivity of T for the effect parameter y [21] is:

$$S_T^y = \frac{1}{T} . \frac{\partial T}{\partial y}$$ (2)

In a linear approximation (1st order Taylor expansion) [21], we obtain:

$$T_y = T_0 \left(1 + S_T^y . y\right)$$ (3)

where T_0 is the delay time of the response signal from the reflector, and T_y is the delay time when measuring the y parameter.

The variation ΔT of a time delay T_0 is:

$$\Delta T = T_y - T_0 = T_0 . S_T^y . y$$ (4)

Measuring the time delay between transmitted and received signals can be done in a variety of methods. Figure 1(b), the functional relationship of the temperature T and the phase shift between the peaks of the first and second reflections are depicted by:

$$\varphi_{2-1}(T) = \varphi_{2-1}\left(T_{ref}\right) . \left[1 + TCD * (T - T_{ref})\right]$$ (5)

where T_{ref} is the reference temperature (or room temperature) and TCD is the temperature hysteresis coefficient of the substrate material. This phase shift is affected by environmental factors (temperature, pressure, humidity [22]), and the position of the reflectors [5]. Gruber *et al.* [15] modeled SAW on MATLAB to calculate $tan\varphi$ but did not consider the influence of reflectors.

This paper evaluates the phase shift between the feedback pulses in which we have used the results obtained from the FEM simulation as amplitude, wavelength, and time delay of the reflected waves to build the model and algorithm on MATLAB to calculate the phase shift angle. The details are presented in sections 2.2 and 2.3.

2.2. FEM simulation

Figure 2(a) shows the SAW structure used in the FEM simulation. The SAW has three aluminum reflectors, a substrate made by YZ-LiNbO$_3$, and an IDT. The reflector combines four electrodes. The IDT is bidirectional with 50 pairs of fingers, and the wavelength (λ) is 39.94 μm. In the applications of wireless passive SAW sensors, the reflectors are chosen so that the response signals are as large as possible. As the

thickness of the bars in the reflector increases, the amplitude of the reflected wave also increases [18]. However, increasing the thickness of the fingers of IDT will reduce the resonant frequency [23]. In this paper, we have chosen the thickness of the bars in the first reflector to be equal to the thickness of the IDT fingers. The thickness of the IDT finger and reflector 1 are 2 μm so the ratio gives $h_1/\lambda = 0.05$ [24] and the thickness of the reflectors 2,3 is 4 μm, respectively $h_2/\lambda=0.1$ to increase the amplitude of the 2nd and 3rd reflected waves.

Figure 2(b) shows the cross-sectional view of two IDT fingers, where d is the period of electrodes, a is the distance between the electrodes, h_1 is the thickness of the IDT fingers, and p is the periodicity of a periodic structure. Table 2 indicates the detailed parameters used in the simulation. The center frequency is [25]:

$$f = v/\lambda \tag{6}$$

where v is the velocity of the SAW and λ is the wavelength. The propagation velocity of the surface wave depends on the shear angle of the substrate material or elastic matrix [26] as (7):

$$v = \sqrt{\frac{c_{66}}{\rho}} \text{ (m/s)} \tag{7}$$

where

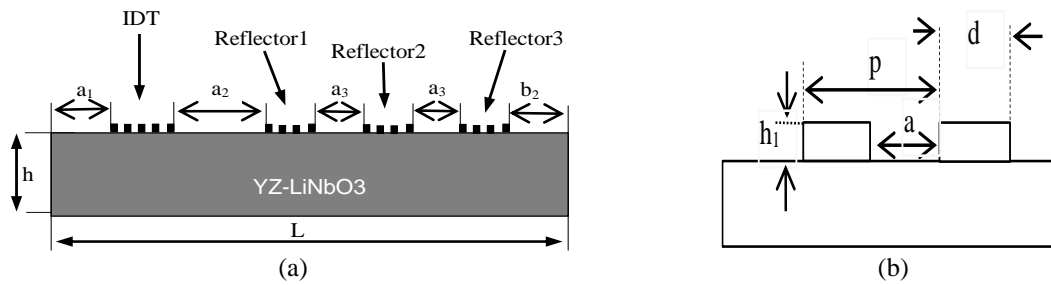$$c_{66} = \frac{c_{11}-c_{12}}{2} \tag{8}$$

Figure 2. The passive wireless SAW structure (a) the 2D structure was used in the FEM simulation and (b) the cross-sectional view of two IDT fingers

With the YZ-LiNbO₃ substrate, coefficients of the elastic matrix, c_{ij}, and density are described in Table 3 [24]. From (7) and (8), we calculated the velocity of wave propagation on the substrate as 3994 m/s and wavelength λ=39.94 μm with the center frequency of 100 Mhz. We test the surface wave propagation velocity during simulation by applying a Dirac delta function to the IDT and then reading the propagating pulse to the first reflector to find the correct center frequency.

Table 2. Geometric parameters used in the FEM simulation

Parameters	Structure 1	Structure 2	Structure 3
The length of the substrate, L_e (μm)	5394	5463.6	5533.2
The number finger of IDT, N	50	50	50
The wavelength, λ (μm)	39.94	39.94	39.94
The thickness of the substrate, h (μm)	400	400	400
The IDT-reflector 1 gap, a_2 (μm)	870	939.6	1009.2
The reflector-reflector gap, a_3 (μm)	452.4	522	591.6
The IDT-left boundary gap, a_1 (μm)	1740	1740	1740
The reflector 3- right boundary gap, b_2 (μm)	1740	1740	1740
The thickness of the IDT fingers and reflector 1, h_1 (μm)	2	2	2
The thickness of the IDT fingers and reflector 2,3, h_2 (μm)	3.99	3.99	3.99

In the structure of SAW one-port with three reflectors simulated FEM as shown in Figure 2(a), to reduce the simulation time in the meshing process, the substrate below the IDTs and reflectors has a thick mesh with 40 elements per wavelength and other regions have a sparse mesh with 10 to 20 elements per

wavelength. With the above meshing, the total number of elements obtained is 41516 and the solving time is 2 μs. To calculate the propagation velocity of the acoustic wave, firstly, we put the Dirac pulse in the IDT and read the transmitting pulse to the first reflector. After that, we take a fast Fourier transform FFT to get a frequency response at f=102.4 Mh– as shown in Figure 3. With this frequency, from (1.4), we can calculate the velocity of the transmitting wave as 3702.72 m/s.

With the received frequency, the AC voltage applied to the IDT is $2 * \cos(2\pi * 102.4 * 10^6 * t) rect(t - 50 * 10^9)$, where t is the time and $rect(x) = 1$, when $0 < x < 1$. Otherwise, $rect(x) = 0$; τ is the width of the Dirac pulse. In Figure 2, the right boundary gap and the reflector–the left boundary gap and the IDT are calculated to evade the reflected waves from boundaries since we only care about the reflected waves from these reflectors. Solution time is 2 μs ensures that the response is received from the reflectors.

Table 3. Elastic matrix coefficient (GPa) and density $\rho(10^3 \text{ kg/m}^3)$ of YZ-LiNbO$_3$

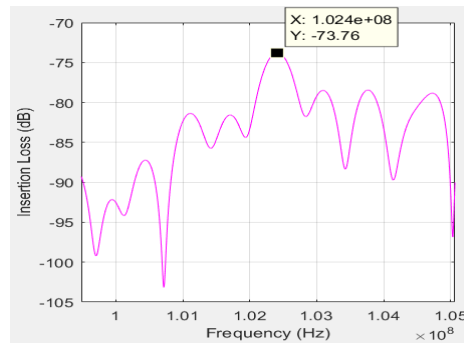| c_{11}	c_{12}	c_{13}	c_{33}	c_{44}	c_{14}	ρ
203	53	75	245	60	9	4.7

Figure 3. Frequency response when applying the Dirac pulse to the IDT

2.3. The modeling on MATLAB

The one-port SAW delay line sensor is not able to model with only one port, it has been described as a two-port system on MATLAB, consisting of input and output, but with the same behavior, as Figure 4. When putting a voltage to the IDT, due to the piezoelectric effect described in section 2.1, a SAWs will propagate to the reflectors 1-3. Because the reflectors are located at different positions on the piezoelectric substrate, the reflected waves will be obtained at different times τ_1, τ_2, and τ_3. Figure 4 shows the results from response pulses in the FEM simulation as $Gain_i$, l_i, and τ_i (l_i are the length of the reflected waves, and $gain_i$ represents the amplitude loss of the reflected waves, respectively, ($i = 1 \div 3$). These results are put in the block diagram of the reception and transmission model at IDT with three reflectors of SAW on MATLAB/Simulink. Evaluating the signal delay allows for the calculation desired measurement quantity. Figure 5 shows the MATLAB/Simulink model for calculating phase parameters.

The voltage applied to the IDT is:

$$u(t) = A * \cos(\omega * t) \text{ (V)} \tag{9}$$

where A is the input voltage amplitude, $A = 2(V)$; ω is the frequency of the input signal, $\omega = 2 * \pi * 102.4 * 10^6 (rad/s)$.

The sum of response signals from three reflectors at the output (Figure 4) is:

$$\sum_{i=1}^{n} A * A_i * \cos(\omega * (t - \tau_i) + \theta) * \prod(t - \tau_i) \tag{10}$$

where A_i is the amplitude loss for the reflectors after passing the ith reflector, respectively; n is the number of reflectors, $n= 3$; τ_i is the delay time corresponding to the ith reflector.
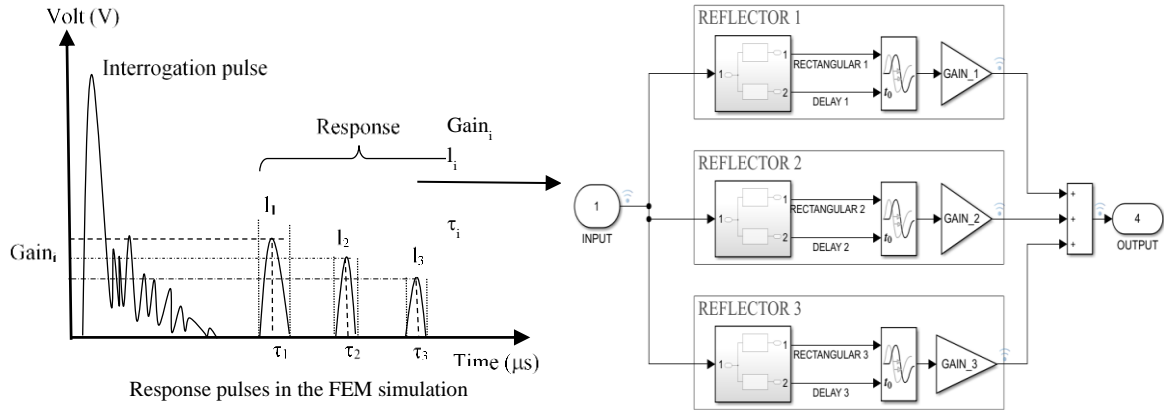
Figure 4. The results in the FEM simulation put in the block diagram of SAW on MATLAB/Simulink
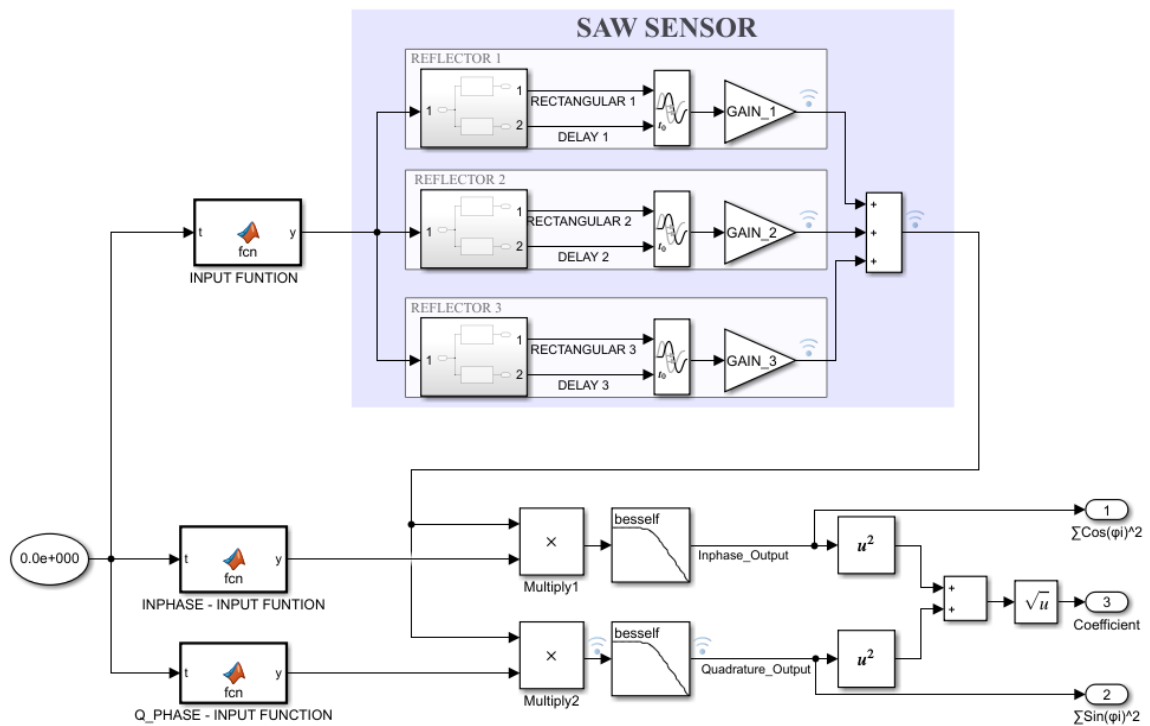

Figure 5. The Simulink model of calculating phase parameter

3. RESULTS AND DISCUSSION

Figure 6 indicates the amplitude of the input wave on the IDT and reflected waves from the first, the second, and the third reflector in FEM simulation. These reflected waves reach the maximum amplitude at the times τ_1, τ_2, and τ_3, and have lengths l_1, l_2, and l_3, respectively. In the simulated structure, the maximum amplitude of the response pulses from the first, the second and the third reflector are 0.05604 (V), 0.02687 (V) and 0.01811 (V) at the times τ_1=0.487 (μs), τ_2=0.806 (μs), and τ_3=1.132 (μs), respectively. The times when the IDT receives the reflected waves according to the theoretical calculation are τ_11, τ_21, and τ_31. Where τ_11=(L_e/2+2*a_2)/v=0.5157(μs); τ_21=(L_e/2+(a_2+a_3+7*d)*2)/v=0.798 (μs), and τ_31=(L_e/2+(a_2+2*a_3+14*d)*2)/v=1.054(μs), respectively, where L_e is the length of IDT, L_e=(4*N-1)*d (μm). The times to reach the maximum reflected voltage amplitudes in the simulation are approximate to the values in the theoretical, and the time value in simulation is shorter due to the decrease of the velocity in propagation [27]. The comparison of the times to receive the maximum reflected voltage amplitudes between simulation and theoretical calculation with three structures is in Table 4.
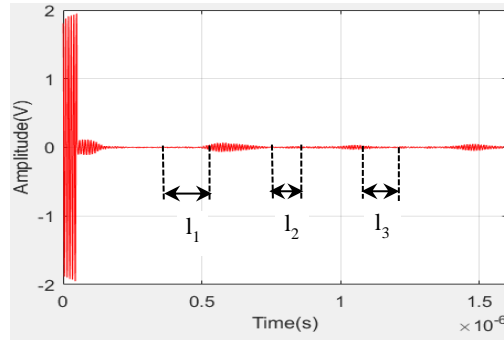
Figure 6. The amplitude of input and in the FEM simulation

Table 4. Comparison the simulation results with the theories for time to reach the largest amplitude of reflected waves in three structures

Parameters	SAW1	SAW2	SAW3
a_2 (μm)	870	939.6	1009.2
a_3 (μm)	452.4	522	591.6
τ_1(μs)	0.487	0.526	0.596
τ_{11}(μs)	0.5157	0.5533	0.5909
τ_2 (μs)	0.806	0.8928	1.04
τ_{22} (μs)	0.798	0.8732	0.9942
τ_3 (μs)	1.132	1.268	1.475
τ_{33} (μs)	1.0542	1.1673	1.2813

With the results shown in Table 4, the difference in time to reach the maximum amplitude of response waves between the simulation and theory at the third reflector is appropriate because the waves propagating from the IDT to the third reflector were weaker and the velocity of the waves decreaseed. The difference in distances of these three structures simulated describes the change of material structure in the measurement of physical quantities with the distance between the IDT and the first reflector, and between these reflectors in the first structure are the smallest, respectively in the third structure are the largest. Table 5 shows results obtained from the FEM simulation, and these results are used to input model of the reader in MATLAB, where $Gain_i$, τ_i, and l_i are the amplitude loss, the time delay, and the length of the reflected waves, respectively of the structures of SAW1, SAW2, SAW3. Figure 7 shows the signals received from three reflectors of the first structure. The output of SAW is a copy sequence of attenuated and delayed from the input.

Table 5. The synthesis of results from the FEM simulation

Parameter	SAW1	SAW2	SAW3
$Gain_1$ (V)	0.05604	0.05569	0.05708
$Gain_2$ (V)	0.02687	0.009257	0.03264
$Gain_3$ (V)	0.01811	0.03811	0.05088
τ_1 (μs)	0.487	0.526	0.596
τ_2 (μs)	0.806	0.8928	1.04
τ_3 (μs)	1.132	1.268	1.475
l_1 (μs)	0.236	0.25	0.2112
l_2 (μs)	0.02236	0.13	0.1369
l_3 (μs)	0.126	0.065	0.175

The product of (9) and (10) is:

$$S_{im}(t) = A * \cos(\omega * t) * \sum_{i=1}^{n} A * A_i * \cos(\omega * (t - \tau_i) + \theta) * \prod(t - \tau_i) \qquad (11)$$

in (10) corresponding to the input signal of analog filter 1, described in Figure 8(a).

Shifting the phase of (9) and (10) by 90 degrees, then multiplying them together (corresponding to the input signal of analog filter2), we get:

$$SQm(t) = A * cos(\omega * t - \frac{\pi}{2}) * \sum_{i=1}^{3} A * A_i * cos(\omega * (t - A_i) + \theta) * \prod(t - \tau_i) \qquad (12)$$

Figure 8(b) shows the graph of $S_{Qm}(t)$. From formula:

$$\cos(x) * \cos(y) = \frac{1}{2} \left[\cos(x+y) + \cos(x-y) \right]$$

In (11) becomes:

$$S_{Im}(t) = A^2 * A_i * \sum_{i=1}^{3} \prod(t - \tau_i) * \frac{1}{2} * \left[\cos(\omega * t + \omega * (t - \tau_i) + \theta) + \cos(\omega \tau_i + \theta) \right] \quad (13)$$
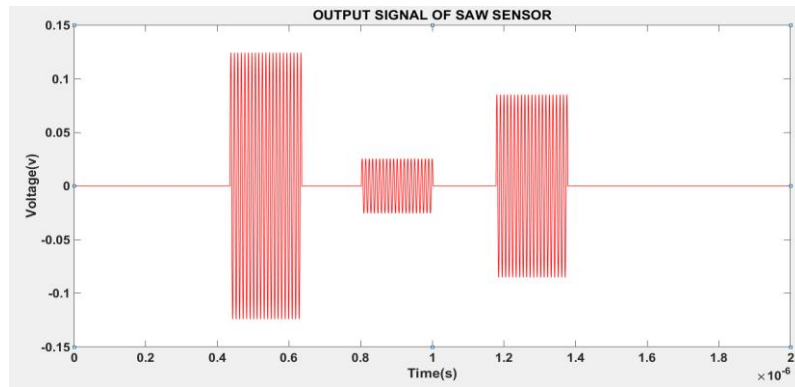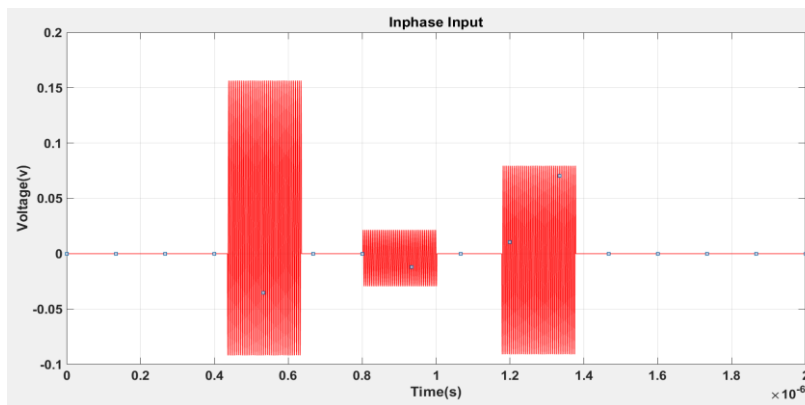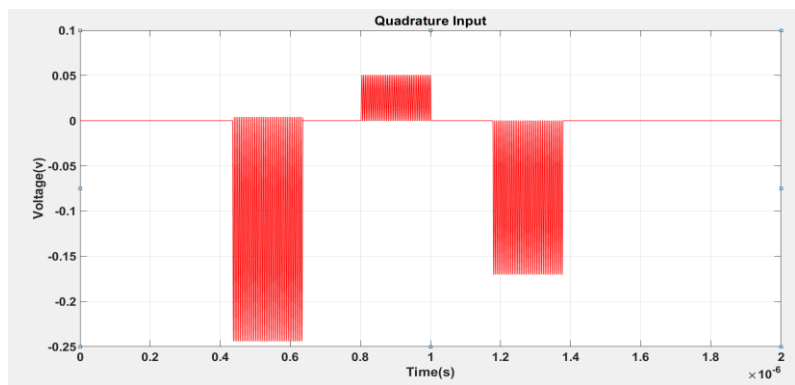

Figure 7. Response signals from 3 reflectors of the SAW1

(a)

(b)

Figure 8. Input signals of analog for SAW1 for (a) the input signal of the filter1 and (b) the input signal of the filter2

and (12) becomes:

$$S_{Qm}(t) = A^2 * A_i * \sum_{i=1}^{3} \prod(t - \tau_i) * \frac{1}{2} * [\cos(\omega * t - \frac{\pi}{2} + \omega * (t - \tau_i) + \theta + \cos(\omega \tau_i + \theta)] \quad (14)$$

after low pass filtering $S_{Im}(t)$ and $S_{Qm}(t)$ we get the signals in Figures 9(a) and 9(b), respectively with (15), and (16) where the phase shift can be calculated by sampling the signal levels of in-phase and quadrature channels.

$$S_{Im}(t) = \sum_{i=1}^{3} C_i * \prod(t - \tau_i) * \cos(\omega \tau_i + \theta) \quad (15)$$

$$S_{Qm}(t) = \sum_{i=1}^{3} C_i * \prod(t - \tau_i) * \sin(\omega \tau_i + \theta) \quad (16)$$

Where $C_i = \frac{1}{2} * A^2 * A_i$.

From (15), (16), $S_{Im}(t)$ and $S_{Qm}(t)$ consist of separate segment independent sine and cosine signals, we consider any component corresponding with the coefficient *i*.

$$S_{Imi} = C_i * \cos(\omega \tau_i + \theta) \quad (17)$$

$$S_{Qmi} = C_i * \sin(\omega \tau_i + \theta) \quad (18)$$
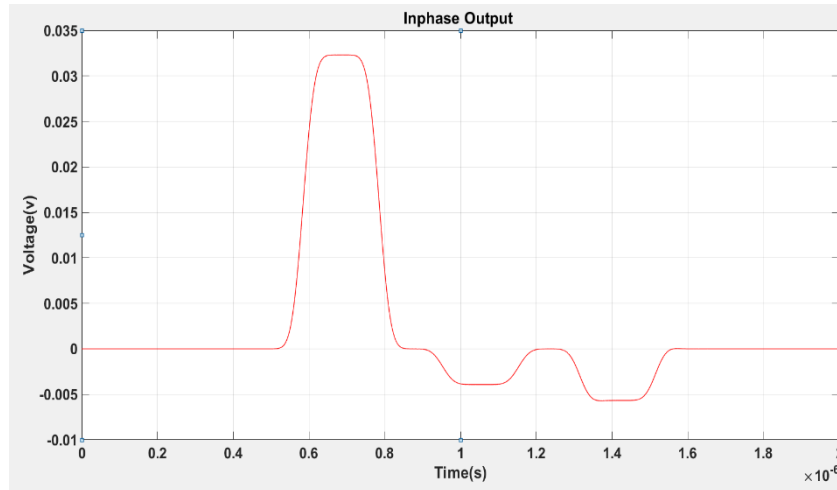
(a)
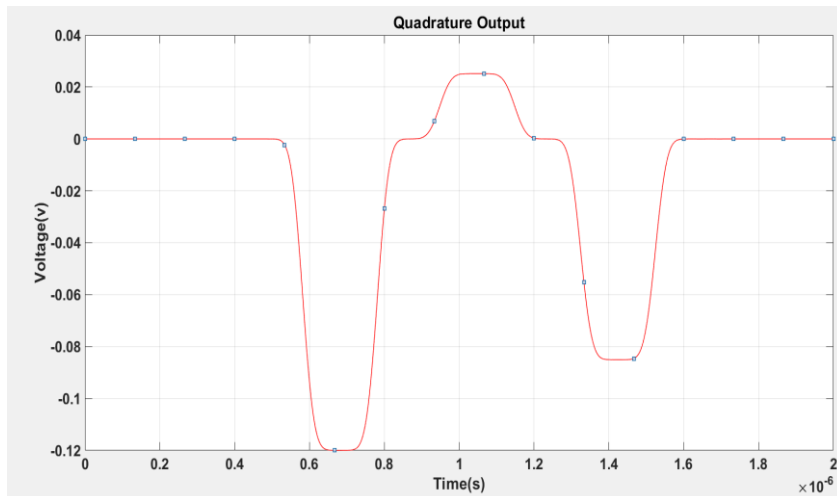
(b)

Figure 9. Low-pass filter in-phase quadrature of SAW1 for (a) in-phase and (b) quadrature

From (17) and (18) we get:

$$C_i = \sqrt{S_{Im}^2 i + S_{Qm}^2 i}$$ (19)

where C_i is the coefficient of reflectors in output. The output signal amplitudes from three reflectors are described in Figure 10.
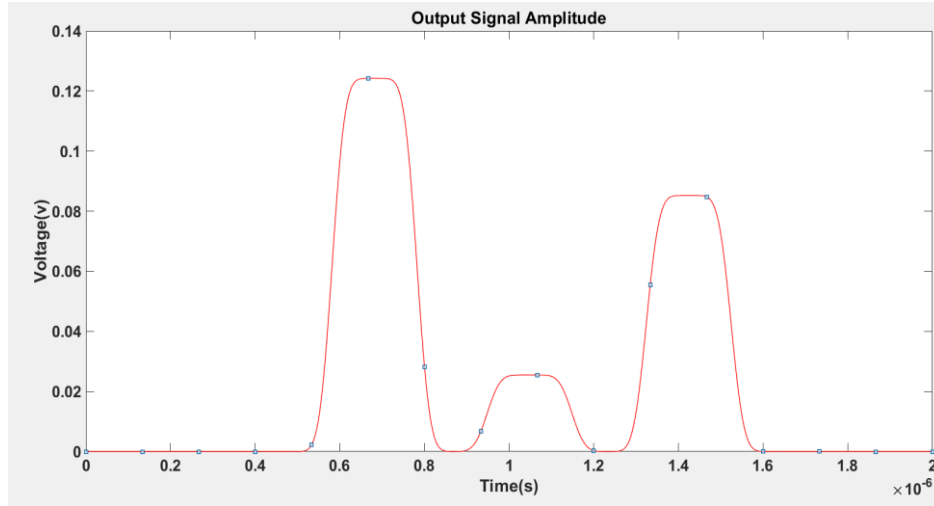

Figure 10. The output signal amplitudes of three reflectors

With the parameters of structure 1 in Table 4, let the phase delay angle of the reflector 1, 2, 3 be φ_1 φ_2, and φ_3 respectively. From MATLAB/Simulink we get $sin(\varphi_i)$ and $cos(\varphi_i)$. Because φ_i is larger than 2π, $arccos(\varphi_i)$ will give the incorrect value of φ_i. In this paper, the distance of the first-to-second reflector (d_{21}) is equal to the distance of the second- to-third reflector (d_{32}), we get $\tau_{21} = \tau_2 - \tau_1$ and $\tau_{32} = \tau_3 - \tau_2$, where τ_{21} is the time delay between reflector 1 and reflector 2, τ_{32} is the time delay between reflector 2 and reflector 3. Because $d_{32} = d_{21}$, when the temperature or physical parameters change, the difference $\varphi_{32} = \varphi_{21}$ is very small and it is in the range of 2π which calculates $arccos(\varphi_{32} - \varphi_{21})$ accurately. We have the (20):

$$\begin{aligned}
sin[(\varphi_3 &- \varphi_2) - (\varphi_2 - \varphi_1)] \\
&= sin(\varphi_3 - \varphi_2) * \cos(\varphi_2 - \varphi_1) - cos(\varphi_3 - \varphi_2) * \sin(\varphi_2 - \varphi_1) \\
&= [\, sin(\varphi_3) * (cos(\varphi_2))^2 * \cos(\varphi_1) - cos(\varphi_3) * \sin(\varphi_2) * cos(\varphi_2) \\
&\quad * cos(\varphi_1) + sin(\varphi_3) * cos(\varphi_2) * \sin(\varphi_2) * \sin(\varphi_1) - cos(\varphi_3) \\
&\quad * (sin(\varphi_2))^2 * \sin(\varphi_1)] \\
&\quad - [\, cos(\varphi_3) * cos(\varphi_2) * \sin(\varphi_2) * cos(\varphi_1) + sin(\varphi_3) * (sin(\varphi_2))^2 \\
&\quad * cos(\varphi_1) - cos(\varphi_3) * (cos(\varphi_2))^2 * sin(\varphi_1) - sin(\varphi_3) * sin(\varphi_2) \\
&\quad * cos(\varphi_2) * \sin(\varphi_1)]
\end{aligned}$$ (20)

where $sin(\varphi_1)$, $\cos(\varphi_1)$, $sin(\varphi_2)$ $cos(\varphi_2)$ $sin(\varphi_2)$, $cos(\varphi_3)$ are obtained from the model on MATLAB, we get $sin[(\varphi_3 - \varphi_2) - (\varphi_2 - \varphi_1)] = 0.9754$ so $[(\varphi_3 - \varphi_2) - (\varphi_2 - \varphi_1)] = 4.49$. Similarly, we have phase values for SAW2 and SAW3. Table 6 shows the phase shift angles of three structures.

Table 6. The phase shift angles of three structures of SAW

Sensor	[(φ3-φ2) – (φ2 –φ1)]
SAW1	4.49
SAW2	5.39
SAW3	5.78

Table 6 shows that as the distance between the IDT and the reflectors increases, the phase shift angles also increase. The effect of physical factors such as temperature, stress, and pressure on the sensor cause changes in the propagation length and velocity of SAW, which change the time delay and the phase angle in the reflection [24].

4. CONCLUSION

In this paper, we combine the parameters from the SAW model of FEM simulation with blocks of the SAW model in MATLABwith three structures corresponding to three different positions of the reflectors, which shows the influence of the measurands on the sensor. To eliminate the ambiguity when the phase shift exceeds 360 degrees, we used the time delay τ_{32}, between the 3rd and 2nd reflectors, and the delay time, τ_{21}, between the 2nd and 1st reflectors. We propose an algorithm to calculate the phase shift between the reflected pulses, with the increasing distance of the position between the IDT and the first reflector as 870 micrometers, 939.6 micrometers, and 1009.2 micrometers, corresponding to phase angles 4.49 degrees, 5.39 degrees, and 5.78 degrees also increased gradually. The combination of simulation on two softwares is of great significance in manufacturing and testing the reader of the passive wireless SAW sensors.

REFERENCES

[1] R. Fachberger, G. Bruckner, R. Hauser, and L. Reindl, "Wireless SAW based high-temperature measurement systems," in *2006 IEEE International Frequency Control Symposium and Exposition*, Jun. 2006, pp. 358–367, doi: 10.1109/FREQ.2006.275412.

[2] R. Hauser *et al.*, "A wireless SAW-based temperature sensor for harsh environment," *2004 IEEE SENSORS*, vol. 2, pp. 860–863, Oct. 2004, doi: 10.1109/ICSENS.2004.1426306.

[3] K. Stroganov, T. Kronidov, B. Luylin, V. Kalinin, and V. Plessky, "SAW temperature sensors for electric power transmission lines," in *2014 European Frequency and Time Forum (EFTF)*, Jun. 2014, pp. 157–159, doi: 10.1109/EFTF.2014.7331452.

[4] A. Binder, G. Bruckner, N. Schobernig, and D. Schmitt, "Wireless Surface Acoustic Wave Pressure and Temperature Sensor With Unique Identification Based on $\rm LiNbO_3$," *IEEE Sensors Journal*, vol. 13, no. 5, pp. 1801–1805, May 2013, doi: 10.1109/JSEN.2013.2241052.

[5] W. Wang, K. Lee, S. Yang, and I. Park, "Design Optimization of SAW Pressure Sensor with Equivalent Circuit Model," *Sensors and Materials*, vol. 18, no. 6, pp. 301–312.

[6] B. Donohoe, D. Geraghty, and G. E. O'Donnell, "Wireless Calibration of a Surface Acoustic Wave Resonator as a Strain Sensor," *IEEE Sensors Journal*, vol. 11, no. 4, pp. 1026–1032, Apr. 2011, doi: 10.1109/JSEN.2010.2070492.

[7] V. Kalinin, A. Leigh, A. Stopps, and S. B. Hanssen, "SAW torque sensor for marine applications," in *2017 Joint Conference of the European Frequency and Time Forum and IEEE International Frequency Control Symposium (EFTF/IFCS)*, Jul. 2017, pp. 347–352, doi: 10.1109/FCS.2017.8088889.

[8] B. Li, O. Yassine, and J. Kosel, "A Surface Acoustic Wave Passive and Wireless Sensor for Magnetic Fields, Temperature, and Humidity," *IEEE Sensors Journal*, vol. 15, no. 1, pp. 453–462, Jan. 2015, doi: 10.1109/JSEN.2014.2335058.

[9] F. Lurz, T. Ostertag, B. Scheiner, R. Weigel, and A. Koelpin, "Reader Architectures for Wireless Surface Acoustic Wave Sensors," *Sensors*, vol. 18, no. 6, Jun. 2018, doi: 10.3390/s18061734.

[10] G. Bruckner and J. Bardong, "Wireless Readout of Multiple SAW Temperature Sensors," *Sensors*, vol. 19, no. 14, Jan. 2019, doi: 10.3390/s19143077.

[11] C. Fu *et al.*, "Design and Implementation of 2.45 GHz Passive SAW Temperature Sensors with BPSK Coded RFID Configuration," *Sensors*, vol. 17, no. 8, Aug. 2017, doi: 10.3390/s17081849.

[12] S. Krishnamurthy, B. J. Bazuin, and M. Z. Atashbar, "Wireless SAW sensors reader: architecture and design," in *2005 IEEE International Conference on Electro Information Technology*, May 2005, p. 6, doi: 10.1109/EIT.2005.1626992.

[13] A. Pohl, G. Ostermayer, C. Hausleitner, F. Seifert, and L. Reindl, "Wavelet transform with a SAW convolver for sensor application," in *1995 IEEE Ultrasonics Symposium. Proceedings. An International Symposium*, Nov. 1995, vol. 1, pp. 143–146 vol. 1, doi: 10.1109/ULTSYM.1995.495557.

[14] F. Schmidt, O. Sczesny, C. Ruppel, and V. Magori, "Wireless interrogator system for SAW-identification-marks and SAW-sensor components," in *Proceedings of 1996 IEEE International Frequency Control Symposium*, Jun. 1996, pp. 208–215, doi: 10.1109/FREQ.1996.559845.

[15] C. Gruber, A. Binder, and M. Lenzhofer, "Fast Phase Analysis of SAW Delay Lines," in *Internet of Things. IoT Infrastructures*, Cham, 2016, pp. 373–382, doi: 10.1007/978-3-319-47075-7_42.

[16] N. Y. Kozlovski, D. C. Malocha, and A. R. Weeks, "A 915 MHz SAW Sensor Correlator System," *IEEE Sensors Journal*, vol. 11, no. 12, pp. 3426–3432, Dec. 2011, doi: 10.1109/JSEN.2011.2159856.

[17] L. Reindl, G. Scholl, T. Ostertag, C. C. W. Ruppel, W.-E. Bulst, and F. Seifert, "SAW devices as wireless passive sensors," in *1996 IEEE Ultrasonics Symposium. Proceedings*, Nov. 1996, vol. 1, pp. 363–367, doi: 10.1109/ULTSYM.1996.583993.

[18] N. T. Ha, T. M. Hung, N. H. Nam, N. T. Huong, L. C. Thanh, and H. S. Hong, "A FEM simulation of the influence of the reflector on the response of the passive wireless SAW structure," *Vietnam Japan Microwave 2017 Conference*, pp. 99–103, 2017.

[19] A. E. Fatimi, S. Bri, and A. Saadi, "An ultra wideband antenna for Ku band applications," *International Journal of Electrical and Computer Engineering (IJECE)*, vol. 9, no. 1, Feb. 2019, doi: 10.11591/ijece.v9i1.pp452-459.

[20] L. Reindl, G. Scholl, T. Ostertag, H. Scherr, U. Wolff, and F. Schmidt, "Theory and application of passive SAW radio transponders as sensors," *IEEE Transactions on Ultrasonics, Ferroelectrics, and Frequency Control*, vol. 45, no. 5, pp. 1281–1292, Sep. 1998, doi: 10.1109/58.726455.

[21] A. Pohl, "A review of wireless SAW sensors," *IEEE Transactions on Ultrasonics, Ferroelectrics, and Frequency Control*, vol. 47, no. 2, pp. 317–332, Mar. 2000, doi: 10.1109/58.827416.

[22] T. J. Harpster, B. Stark, and K. Najafi, "A passive wireless integrated humidity sensor," in *Technical Digest. MEMS 2001. 14th IEEE International Conference on Micro Electro Mechanical Systems (Cat. No.01CH37090)*, Jan. 2001, pp. 553–557, doi: 10.1109/MEMSYS.2001.906601.

[23] W. Connacher *et al.*, "Micro/nano acoustofluidics: materials, phenomena, design, devices, and applications," *Lab Chip*, vol. 18, no. 14, pp. 1952–1996, Jul. 2018, doi: 10.1039/C8LC00112J.

[24] N. T. Ha, P. D. Hung, H. S. Hong, and N. T. Truyen, "A study of the effect of IDTs and input signals on the amplitude of propagation waves of the passive SAW structure," in *2017 International Conference on Information and Communication Technology Convergence (ICTC)*, Oct. 2017, pp. 453–457, doi: 10.1109/ICTC.2017.8191018.

[25] C. Campbell, *Surface Acoustic Wave Devices and Their Signal Processing Applications*. Academic Press, 2012.

[26] B. A. Auld, *Acoustic fields and waves in solids*. Springer-Verlag Berlin Heidelberg, 1973.

[27] K.-Y. Hashimoto, *Surface Acoustic Wave Devices in Telecommunications: Modelling and Simulation*, 2000th edition., vol. 116. Berlin ; New York: Springer, 2000.

BIOGRAPHIES OF AUTHORS

Nguyen Thu Ha 🆔 ⬛ SC ↻ graduated in the field of Instrumentation and Industrial Informatics in 2001 and completed a master's degree in Control Engineering and Automation in 2007 at Hanoi University of Science and Technology. Since 2001, she is working as a lecturer at the Faculty of Electrical Engineering Technology and studying as a Ph.D. student at the School of Electrical and Electronic Engineering, Hanoi University of Science and Technology, Vietnam. Her main research areas are SAW, passive wireless SAW sensors, and wireless sensor networks. She can be contacted at emai: nguyen.ha@haui.edu.vn.

Trinh Van Thai 🆔 ⬛ SC ↻ is now a 4th-year student under the supervision of Assoc. Prof. Hoang Si Hong at School of Electrical and Electronic Engineering, Hanoi University of Science and Technology. His current research interests are focused on the SAW and wireless sensor networks. He can be contacted at email: trinhvanthai190820@gmail.com.

Thanh Long Cung 🆔 ⬛ SC ↻ received his B. Eng degree in Measurement and Automatic Control, in 2000, and his M.Sc degree in Measurement and Control Systems, in 2002, at Hanoi University of Science and Technology, Vietnam. He received his Ph.D. degree in Electronics-Electrotechnique-Automation, in 2012, at Ecole Normale Superieure Paris-Saclay, France. He is currently a researcher/lecturer at the School of Electrical Engineering, Hanoi University of Science and Technology. His research interests include electromagnetic non-destructive testing/evaluation, human emotion recognition, sensors, and signal processing. He can be contacted at email: long.cungthanh@hust.edu.vn.
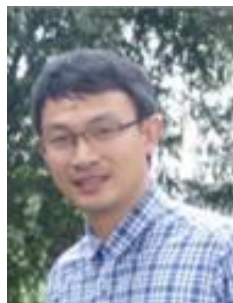
Hoang Si Hong 🆔 ⬛ SC ↻ received his B.E and M.E degree in the School of Electrical Engineering from Hanoi University of Technology, Hanoi, Vietnam, in 1999 and 2001, respectively, and his Ph.D. degree from the University of Ulsan, Ulsan, Korea, in 2010. Now, he is an Associate Professor at the School of Electrical and Electronic Engineering, Hanoi University of Science and Technology, Hanoi, Vietnam. His research interests include piezoelectric material, SAW sensor, passive wireless sensor, and harvesting energy. He can be contacted at email: hong.hoangsy@hust.edu.vn.